ELSEVIER

PII: S0032-3861(97)00455-2

Polymer Vol. 39 Nos. 8–9, pp. 1533–1538, 1998

0032-3861/97/$17.00+0.00

Phase behaviour and morphology development in a blend of isotactic polypropylene and hydrogenated poly(styrene-*co*-butadiene)

Nobuyoshi Otsuka[a], Ying Yang[a], Hiromu Saito[a,*], Takashi Inoue[a] and Yasuhiko Takemura[b]

[a]*Department of Organic and Polymeric Materials, Tokyo Institute of Technology, Ookayama, Megoru-ku, Tokyo 152, Japan*

[b]*Yokkaichi Research Laboratories, Japan Synthetic Rubber Co., Ltd, 100 Kawajiri, Yokkaichi 510, Japan*

(Received 10 February 1997; revised 1 May 1997)

A hydrogenated poly(styrene-*co*-butadiene) (hSBR) was found to be miscible with isotactic polypropylene (iPP) above the melting point of iPP. The mixture was phase-separated at lower temperatures, i.e. the iPP/hSBR blend exhibited upper critical solution temperature (*UCST*) type phase behaviour (*UCST* ≈ 100°C). The *UCST* phase behaviour was determined by time-resolved light scattering analysis. In the quenched 50/50 blend, a microphase-separated structure of hSBR domains, having a diameter of 20 nm, dispersed quite regularly in an iPP-rich matrix (periodic distance ≈ 40 nm) was observed by transmission electron microscopy. The microphase-separated structure seems to originate from spinodal decomposition below the *UCST* during the quenching process. The formation of large and ordered lamella crystallites was suppressed to yield fine PP crystallites (of size ≈ 8 nm, as estimated by the Sherrer equation). This may be caused by the presence of the hSBR. Thus, the partially miscible impurity (hSBR) produces fine iPP crystallites which can act as crosslink points to provide thermoplastic elastomer-type character to the blend.

(Keywords: isotactic polypropylene; hydrogenated poly(styrene-*co*-butadiene); blend)

INTRODUCTION

Isotactic polypropylene (iPP) is a widely used plastic with easy processing and excellent properties. Blending iPP with other polymers to improve its bulk properties is attracting increasing attention[1–3]. When iPP is blended with a non-crystalline component, the crystalline behaviour of the iPP will be influenced. Depending on the miscibility of the components, the crystalline morphology, such as crystalline size and ordering, and crystalline kinetics will be quite different. Hence, different mechanical properties will result in the blend.

Martuscelli *et al.*[4] found that in iPP/hydrogenated oligo(cyclopentadiene) (HOCP) blend, the spherulite growth rate, the overall crystallization rate and the equilibrium melting point of iPP were drastically depressed by the addition of HOCP. The authors ascribed these results to the miscibility of the two components in the melt. Bodor and co-workers[5] studied the effect of a series of rubber modifiers, such as poly(ethylene-*co*-propylene) (EPR) and polyisoprene, on iPP crystallization. They revealed that incorporation of the modifier reduced the average size of spherulites and inhibited the formation of the less stable β-form crystal. The smaller the average size of spherulites in the blends, the higher was the impact strength at low temperatures. D'orazio *et al.*[6] studied the effect of cross-linking of the rubbery component on the iPP crystallization behaviour in iPP/EPR blends. They found that uncrosslinked EPR did not interfere with the iPP crystallization behaviour very much but just slightly depressed the melting point and reduced the crystallinity, while crosslinked EPR affected the crystallization to form cobweb crystallites surrounding the EPR particles.

Recently, a hydrogenated poly(styrene-*co*-butadiene) (hSBR) was found to be miscible with iPP above the melting point of iPP[7]. This is a rare case of a high-molecular-weight polymer being miscible with iPP. A 50/50 blend of iPP/hSBR prepared by quenching the single-phase melt into room temperature exhibited good strain recovery after large deformation[7,8]. In order to understand the thermoplastic elastomer-type behaviour in the iPP/hSBR blend, we undertook detailed studies on the phase behaviour and morphology development by means of differential scanning calorimetry (d.s.c.), dynamic mechanical analysis (d.m.a.), wide-angle X-ray diffraction (WAXD), small-angle X-ray scattering (SAXS) and transmission electron microscopy (TEM).

EXPERIMENTAL

The iPP and hSBR used in this study were commercial polymers. iPP was supplied by Mitsui Toatsu Chemicals Inc. (J3HG; $M_w = 3.5 \times 10^5$ and $M_n = 5 \times 10^4$, where M_w and M_n are weight-average and number-average molecular weight, respectively). hSBR was supplied by Japan Synthetic Rubber Co. Ltd (Dynaron 1320 P; $M_w = 3 \times 10^5$, styrene content = 10%).

The iPP and hSBR were melt-mixed at 210°C for 5 min in a miniature moulder (Mini-Max, model CS-183MMX, Custom Scientific Instruments, Inc.). The blend ratio was

* To whom correspondence should be addressed

varied; however, most of the experiments reported below were done for a 50/50 blend. The single-phase melt was extruded and the extrudate was compression moulded at 200°C. Then the blend underwent quenching and annealing. The quenching was carried out in water (20°C). For the annealing, two kinds of annealed specimen were prepared. One was a melt-and-annealed specimen: after the blend was melted at 200°C for 5 min, the melt specimen was inserted quickly into a hot stage set at various desired lower temperatures and annealed. The other was a quenched-and-annealed specimen: the quenched specimen was isothermally annealed at 140°C in which only crystallization is expected to proceed.

The blends thus prepared were observed under a polarized optical microscope (Olympus BH-2). For observation of the growth of polypropylene spherulites, iPP and the blend were heated at 200°C for 10 min to destroy the crystalline structures, then the melts underwent a rapid quench to a crystallization temperature by inserting them in the hot stage (Linkam TH600 heating/cooling stage, Linkam Scientific Instruments Ltd) set on the microscope stage. The time variation of the radius of the spherulites during the isothermal crystallization was observed.

Light scattering measurement was carried out with a laser light scattering apparatus. The polarized He–Ne gas laser of 632.6 nm wavelength was applied vertically to the film specimen set on a hot stage at desired temperature. The scattering light was passed through an analyser. We employed two optical geometries; one was the H_v geometry in which the optical axis of the analyser was set perpendicular to that of the polarizer, and the other was the V_v geometry with a parallel set of the two axes. The angular distribution of light scattering intensity was detected by a one-dimensional photometer with a 46-photodiode array (HASC Co., Ltd). The scattering profiles in a time slice of 30 ms were measured at appropriate intervals.

In a differential scanning calorimeter (Seiko SII DSC 6200) the specimens were heated at a heating rate of 20°C min^{-1} in N_2 atmosphere. The melting temperature and the enthalpy of fusion were obtained from the maximum and the area of the endothermic peak, respectively. The crystallinity, X_C, was calculated by:

$$X_C = \frac{\Delta H^*}{\Delta H^0_{iPP}}$$

where ΔH^* is the enthalpy of fusion per gram iPP or that in the blend, and ΔH^0_{iPP} is the heat of fusion per gram of 100% crystalline iPP [= 209 J g^{-1}][9].

Dynamic mechanical behaviour was measured (Toyoseiki Dynamic Mechanical Analyzer) at 100 kHz at a heating rate of 2°C min^{-1}. The temperature dependence of the dynamic loss (tan δ) was obtained.

WAXD patterns were observed in an X-ray diffraction apparatus (Rigaku Denki RU-200) using an image plate (R-AXIS II D). The radiation from the copper anode was reflected from a graphite monochromator to obtain monochromatic Cu K_α radiation with a wavelength of 0.1541 nm. The generator was operated at 40 kV and 100 mA.

Time-resolved SAXS measurements were carried out by using synchrotron radiation at beam line BL-10C in the Photon Factory (National Laboratory for High Energy Physics, Tsukuba). The SAXS employed a point focusing optics with a double flat monochromator followed by a bent cylindrical mirror. The incident beam intensity of 0.1488 nm wavelength was monitored by an ionization chamber for correction of the minor decrease of the primary beam intensity during the measurement. The scattered intensity was detected with a one-dimensional position-sensitive proportional counter (PSPC) with 512 channels. The distance between the sample and the PSPC was about 2 m. The geometry was checked by a chicken tendon collagen, which gave a set of sharp diffractions corresponding to a Bragg spacing of 65.3 nm.

For TEM observation, the specimens were stained with ruthenium tetraoxide (RuO_4) vapour for 0.5 h at 50°C. The stained specimen was microtomed to an ultrathin section of *ca.* 70 nm thickness with an ultracryomicrotome at −70°C. The structure in the section was observed under an electron microscope (JEM-100CX from JEOL).

RESULTS AND DISCUSSION

The temperature dependence of the dynamic loss (tan δ) is shown in *Figure 1*. Pure iPP has a glass transition temperature (T_g; taken as the tan δ peak temperature) at 5°C, whereas that of hSBR is at − 35°C. The quenched blend (blend Q) shows a sharp peak and a shoulder intermediate between those of the constituents. This suggests the existence of two amorphous phases, an iPP-rich phase and a hSBR-rich phase, in which phase mixing of iPP and hSBR takes place. By annealing at 140°C for 80 min, the low T_g shifts to lower temperature, suggesting that phase segregation by crystallization proceeded further during the annealing, i.e. the concentration of iPP decreased in the hSBR-rich amorphous region owing to the crystallization of iPP in the hSBR-rich amorphous region.

As shown in the d.s.c. thermogram of *Figure 2*, the T_g of hSBR is shifted to higher temperature by blending. The glass transition of the hSBR phase in the quenched blend is higher and broader than that in the quenched-and-annealed blend. The result supports the d.m.a. results that hSBR is partially miscible with iPP and that the phase segregation proceeds further by annealing.

Figure 3 shows a TEM micrograph of the blend quenched in water. Dark regions can be assigned to hSBR domains

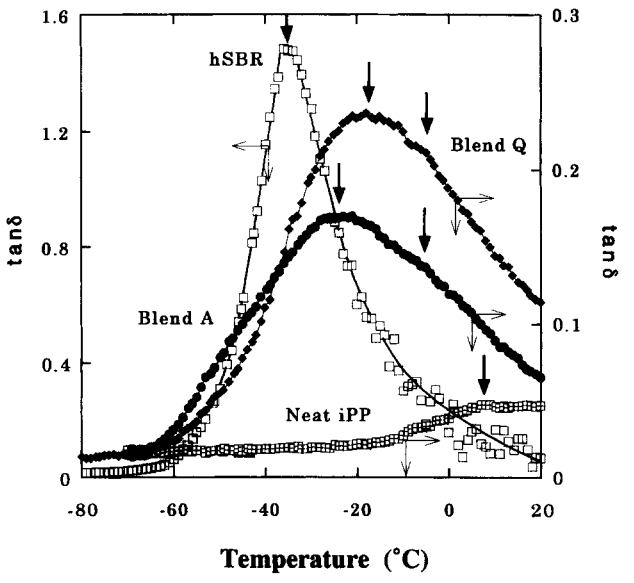

Figure 1 Dynamic loss *versus* temperature curves for the 50/50 iPP/hSBR blends and the component polymers. Blend Q was quenched in water, blend A was quenched-and-annealed blend (blend Q was annealed at 140°C for 80 min), and quenched component polymers

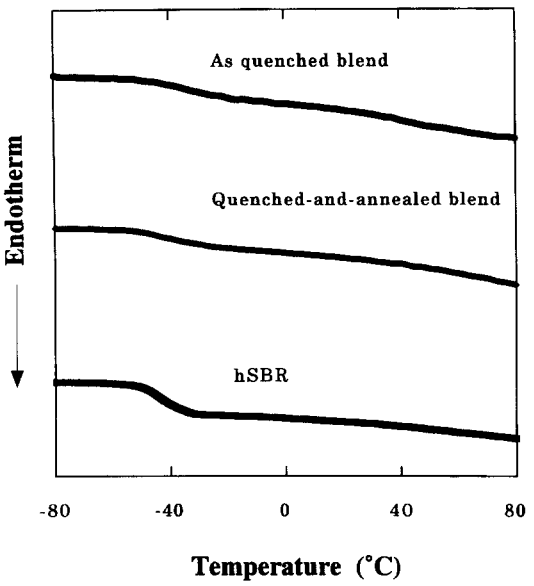

Figure 2 D.s.c. thermograms for the 50/50 iPP/hSBR blends and the component polymers. The thermal treatment conditions for the specimens are the same as those in *Figure 1*

and WAXD analyses even in the quenched blend, as will be discussed later.

The results in *Figures 1–3* imply upper critical solution temperature *UCST* type phase behaviour in the iPP/hSBR blend. Then, we tried to measure the *UCST* phase boundary by the cloud point method. Above the melting temperature (T_m) of iPP, the single-phase nature was confirmed at all compositions; i.e. the phase-separated structure was not observed under optical microscopy even after long annealing ($>$ 10 h). Thus, the *UCST* should be located below the T_m of iPP. Such a *UCST* could be a virtual one and it could not be detected by the cloud point method, which would be disturbed by the crystallization. The virtual *UCST* may be determined by analysing the competition of the liquid–liquid phase separation below *UCST* with crystallization by V_v and H_v light scatterings[10,11]. Unfortunately, in the present systems, no effective information was obtained from the V_v scattering because of the very small difference in refractive index between the constituent polymers and a small correlation length below the wavelength of the light. Effective information was given just at H_v optical alignment.

The H_v scattering profile, the scattered intensity I as a

Figure 3 TEM micrograph of the 50/50 blend quenched in water (stained by RuO_4)

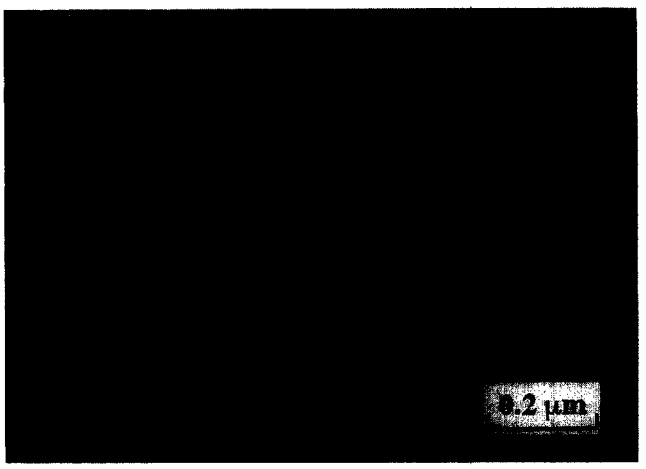

Figure 4 TEM micrograph of the 50/50 blend quenched in water and then annealed at 140°C for 80 min

since the styrene unit is easily stained by RuO_4. It is interesting to note that the domains having a uniform diameter of *ca.* 20 nm are dispersed quite regularly, having a periodic distance of *ca.* 40 nm. The regular phase-separated morphology could be formed by spinodal decomposition arrested at the early stage by the crystallization of iPP.

It is interesting to note that the total area of the dark domains is around 30%. It is very small, if one thinks about the 50/50 composition. The discrepancy suggests that *ca.* 30 parts (among 50 parts) of hSBR segregate out to form the hSBR domains and the remaining 20 parts are in the matrix, probably as an amorphous phase in the iPP-rich matrix as a single-phase mixture with iPP.

Figure 4 shows a TEM micrograph of the blend quenched in water and then annealed at 140°C for 80 min. One sees that hSBR domains are somewhat clustered and that the regularity of the domain arrangement is decreased, suggesting that the arrangement of the hSBR domains was slightly attacked by crystallization of iPP in the hSBR-rich domains during annealing. One sees no crystallites in the TEM micrograph; however, crystals were detected by d.s.c.

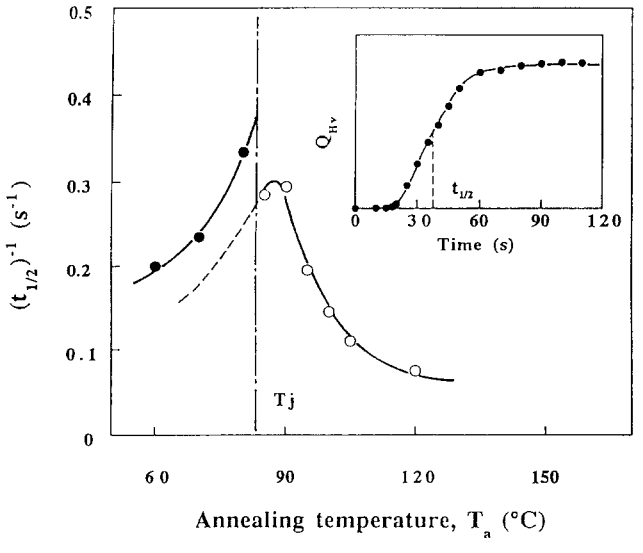

Figure 5 Temperature dependence of crystallization rate, $t_{1/2}^{-1}$. Inset: time variation of H_v light scattering invariant to obtain the rate constant $t_{1/2}$

function of scattering angle θ, was measured at appropriate intervals, after a temperature drop from 210°C ($> T_m$) to the annealing temperature, T_a ($< T_m$). To discuss the crystallization kinetics, it is convenient to employ the integrated scattering intensity, i.e. the invariant Q_{H_v} defined by[12]:

$$Q_{H_v} = \int_0^\infty I(q)q^2 \, dq \propto \langle \delta^2 \rangle$$

where q is the scattering vector, $(4\pi/\lambda)\sin(\theta/2)$, λ being the wavelength in the specimen; and $\langle \delta^2 \rangle$ is the mean-square optical anisotropy. Q_{H_v} increased and then levelled off as shown in the inset of *Figure 5*. Then the half crystallization time, $t_{1/2}$, may be given as the time to reach the 50% level of the attainable Q_{H_v}, as shown in the inset. The inverse of $t_{1/2}$ may be a rate constant of crystallization and it is plotted as a function of annealing temperature T_a in *Figure 5*. In general, the crystallization rate increases as T_a decreases, attains a maximum and then starts to decrease continuously. However, in the present systems, a discontinuity in the $(t_{1/2})^{-1}$ *versus* T_a curve was observed as shown in *Figure 5*. At $T_a = T_j$, the $(t_{1/2})^{-1}$ jumps up to a higher level and then starts to decrease as T_a decreases. Similar results were observed for different compositions.

The jump could be caused by the onset of liquid–liquid phase separation as the T_a is reduced down to the *UCST*. Such an accelerated crystallization has been observed in polyimide/poly(ether sulfone) blends and interpreted in terms of the faster transportation of crystallizable component to the growing front of the crystals, assisted by the 'uphill diffusion' in the spinodal decomposition[13]. In *Figure 5*, the data points above T_j are indicated by open circles and those below T_j by closed circles. The open and closed circles are plotted for various compositions in *Figure 6*. One could draw a solid line between the open and closed circles. The solid line may represent the virtual *UCST* phase boundary.

Under the optical microscope, no visible PP spherulites were found in the quenched blend, while small spheriutes were visible in quenched pure iPP. Even after annealing the quenched specimen at 140°C for 80 min, no spherulites were visible. These observations indicate that crystallization

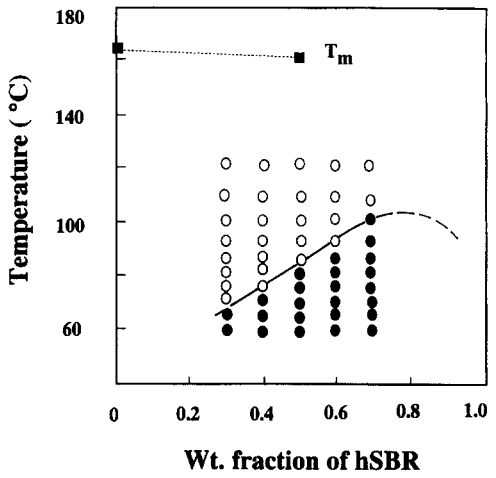

Figure 6 Phase diagram of the iPP/hSBR blend

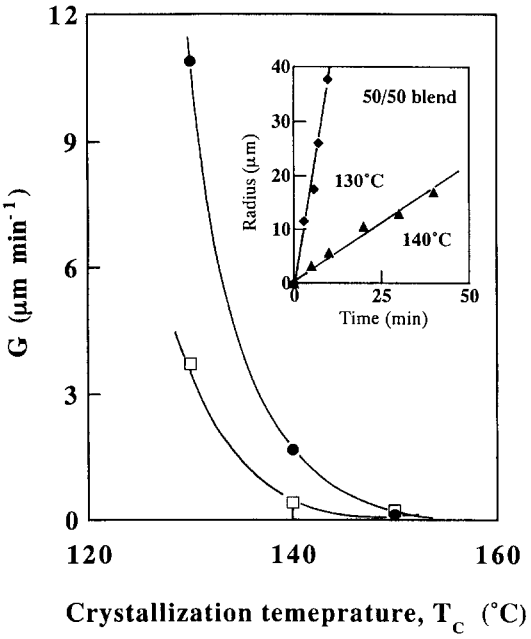

Figure 7 Temperature dependence of the radial growth rate, G, of spherulites: ●, pure iPP; □, 50/50 blend. The values of G were obtained from the slopes of the linear plots in the inset

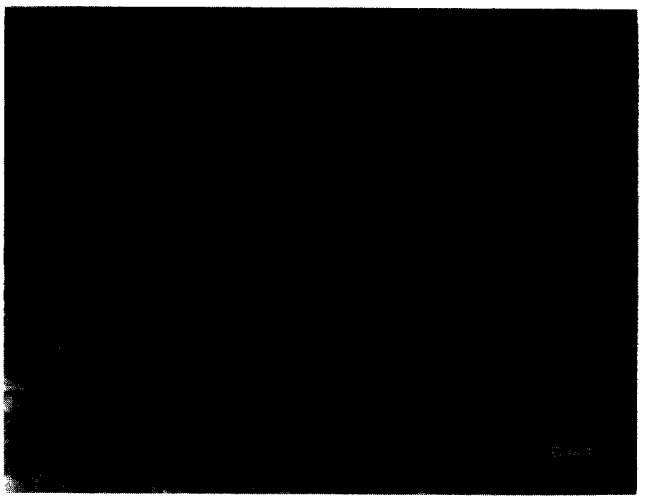

(a)

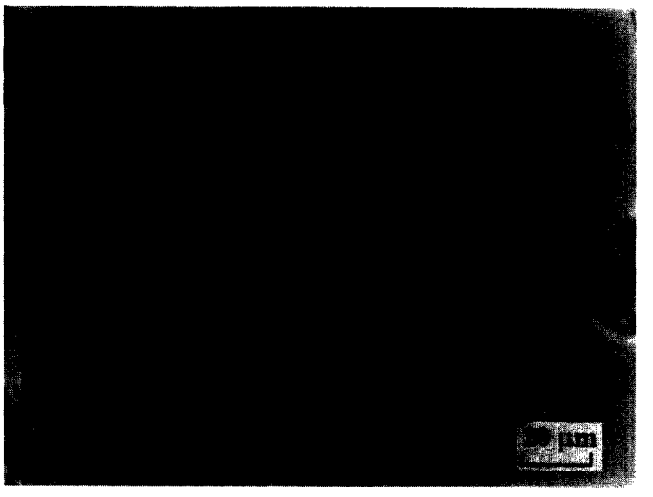

(b)

Figure 8 Optical micrographs of spherulites after crystallization at 140°C for 80 min: (a) pure iPP; (b) 50/50 iPP/hSBR blend

in the matrix phase of the microphase-separated structure in *Figure 3* could not produce the spherulite texture and it just affected the rearrangement of the local structure as shown in *Figure 4*.

In contrast, when pure iPP and the blend were melted at 200°C, quenched directly to 140°C and then isothermally annealed at this temperature, spherulites appeared and grew. Such spherulite growth was observed at various temperatures in the range 120°C to 150°C. The spherulites grew linearly with time, as shown in the inset of *Figure 7*. The growth rate, G, obtained from the slope of the linear growth plot is shown in *Figure 7* as a function of crystallization temperature, T_C. One sees a significant reduction in G by the incorporation of hSBR. The spherulite texture in the blend was also different from that in pure iPP, as typically shown in *Figure 8*. In the case of pure iPP, the spherulite shape was completely round from the very beginning of crystallization, while the spherulites in the blend were irregular in shape, especially at lower crystallization temperatures.

In any case, such spherulite nature was not observed in the quenched blend and the quenched-and-annealed blend as described above, suggesting that the liquid–liquid phase separation below the *UCST* suppressed the formation of spherulites.

The results of thermal analysis by d.s.c. are summarized in *Table 1*. Melting temperature, T_m, was estimated by an intensive endothermic peak at about 160°C. The crystallinity, X_C, was calculated from the area of the endothermic peak. T_m depression in the blend is observed. The depression may be caused by the partial miscibility of iPP and hSBR demonstrated in *Figures 1 and 2*. It is interesting to note that the X_C of PP in the blend is almost same as in pure iPP, suggesting that the impurity (hSBR) in the PP phase only affects the crystalline size and ordering of PP as discussed in the following.

Figure 9 shows the wide-angle X-ray diffraction profiles of the blends. The quenched blend exhibits only four broad diffraction peaks, while the quenched-and-annealed blend clearly shows five diffraction peaks, which corresponds to the monoclinic form of iPP crystallites. The broader diffractions may indicate some defects or smaller crystallites in the blend.

The size of crystallites estimated by the Scherrer equation[14] for the [110] plane was 7.9 nm in the quenched blend and 16.1 nm in the quenched-and-annealed blend. The results suggest that the iPP chains have been rearranged upon annealing and the crystallites can attain a higher ordering with annealing.

Figure 10 shows the time variation of the SAXS profiles in the quenched blend during annealing at 140°C. A small peak is clearly seen for the specimen at $t = 0$ min (as-quenched blend) around the scattering vector at $q = 0.15\ nm^{-1}$, which corresponds to a periodic distance of 40 nm. This peak is assigned to the interdomain spacing of hSBR domains. Annealing induces the appearance of a shoulder at around $q = 0.31\ nm^{-1}$ which grows with time. This shoulder may be assigned to the long spacing of iPP

Table 1 Thermal characterization of crystalline nature in pure iPP and the 50/50 blend

Code	T_m (°C)	Heat of fusion ($J\ g^{-1}$)	X_C (wt%)
Q-blend	161.8	47.3	22.6 (45.2)[a]
A-blend	161.9	58.8	28.1 (56.3)[a]
Q-iPP	164.7	91.9	44.0
A-iPP	164.8	114.0	54.5

Q: quenched in water; A: quenched in water and then annealed at 140°C for 80 min

[a] X_C: per gram of PP

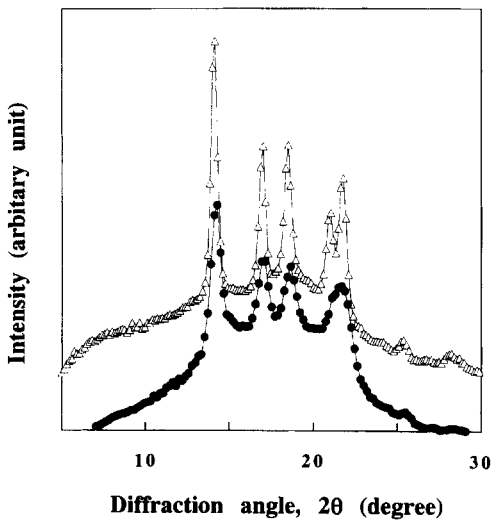

Figure 9 WAXD diffraction curves of the 50/50 blends: ●, quenched in water; △, quenched in water and then annealed at 140°C for 80 min

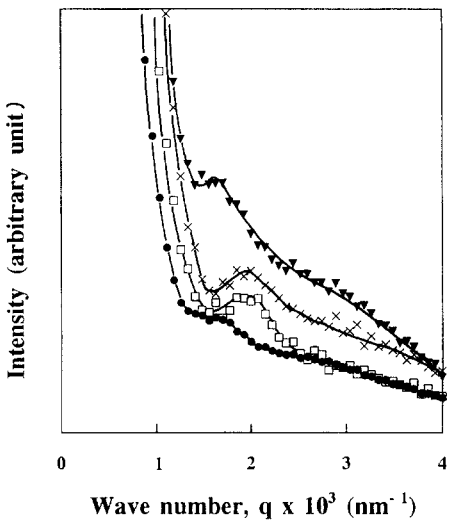

Figure 10 Time variation of the small angle X-ray scattering profile from a 50/50 iPP/hSBR blend during annealing at 140°C: ●, 0 min; □, 15 s; ×, 2 min; ▼, 50 min

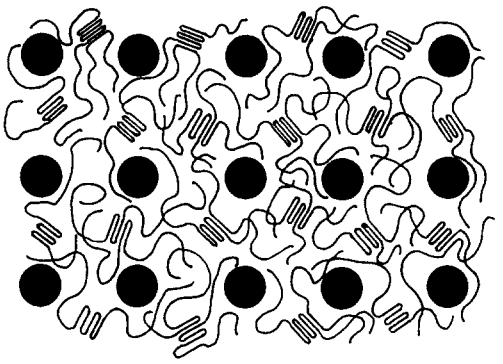

Figure 11 Schematic model for the quenched 50/50 iPP/hSBR blend

crystalline lamellae. The long spacing increases with annealing. The evolution of long spacing in the crystalline structure is accompanied by disappearance of the peak at $q = 0.15\ nm^{-1}$, suggesting disordering in mutual arrangements of domains. Thus, the interdomain spacing seems to be destroyed by ordering in the crystalline morphology of the matrix.

The two T_g values demonstrated by d.m.a., the two-phase morphology observed by TEM and the existence of iPP crystallites identified by d.s.c., WAXD and SAXS suggest that the quenched blend consists of three phases: a segregated hSBR phase, a single-phase mixture of amorphous iPP and hSBR, and an iPP crystalline phase. A morphology model of the quenched blend is shown schematically in *Figure 11*. The hSBR is dispersed as the particle phase and the matrix is a compound phase consisting of fine iPP crystallites and a mixture of amorphous iPP and hSBR.

CONCLUSION

Large crystallites with long spacing and spherulites usually develop in iPP. Such crystalline morphology was found to develop in the iPP/hSBR blend crystallized isothermally at high temperatures. When the blend was quenched in water, this morphology did not appear but finer crystallites with less ordering developed. D.s.c. analysis showed that the crystallinity in the quenched blend was almost same as in pure iPP. The less ordering was shown by WAXD and SAXS. Thus, the miscible impurity (hSBR) in the iPP melt prevents formation of the large and ordered crystallites to yield fine crystallites, which may act as crosslink points to provide the thermoplastic elastomer-type character of the quenched blend. The hSBR domains, formed probably via spinodal decomposition below the *UCST*, seem to suppress spherulite formation, which would be harmful for the thermoplastic elastomer character.

REFERENCES

1. Coran, A. Y., *Handbook of Elastomers—New Developments and Technology*. Mercel Decker, New York, 1988.
2. Morris, H. L., *Handbook of Thermoplastic Elastomers*. Van Nostrand Reinhold, New York, 1979.
3. Wolfe, J. R. Jr., *Thermoplastic Elastomers—A Comprehensive Review*. Hanser Munich, 1986.
4. Martuscelli, E., Canetti, M., Bonfatti, A. M. and Seves, A., *Polymer*, 1991, **32**, 641.
5. Karger, K. J., Kallo, A., Szafner, A., Bodor, G. and Senyei, Z. S., *Polymer*, 1979, **20**, 37.
6. D'orazio, L., Mancarella, C., Martuscelli, E., Sticotti, G. and Ghisellini, R., *J. Appl. Polym. Sci.*, 1994, **53**, 387.
7. Kojima, J., Ishikawa, K., Hashiguchi, Y., Takezaki, Y. and Takemura, Y., presented at ACS Rubber Div., Spring Meeting, 1996, paper #127.
8. Otsuka, N., Saito, H., Inoue, T. and Takemura, Y., *Polym. Prepr., Jpn*, 1995, **44**, 2136.
9. Brandup, S. and Immergut, E. M., *Polymer Handbook*. Interscience, New York, 1975.
10. Tomura, H., Saito, H. and Inoue, T., *Maromolecules*, 1992, **25**, 1611.
11. Svoboda, P., Kressler, J., Chiba, T., Inoue, T. and Kammer, H. W., *Macromolecules*, 1994, **27**, 1154.
12. Koberstein, T., Russell, T. P. and Stein, R. S., *J. Polym. Sci., Polym. Phys. Edn*, 1979, **17**, 1719.
13. Matsuura, M., Saito, H., Nakata, S., Imai, Y. and Inoue, T., *Polymer*, 1992, **33**, 3210.
14. Alexander, L. E., *X-ray Diffraction Method in Polymer Science*. Wiley-Interscience, New York, 1969.